THE JOURNAL OF PHYSICAL CHEMISTRY Letters

Letter

Cite This: J. Phys. Chem. Lett. 2017, 8, 5021-5030

pubs.acs.org/JPCL

# Efficient Method of Designing Stable Layered Cathode Material for Sodium Ion Batteries Using Aluminum Doping

Hari Vignesh Ramasamy,[†] Karthikeyan Kaliyappan,[‡] Ranjith Thangavel,[†] Won Mo Seong,[§] Kisuk Kang,[§] Zhongwei Chen,[‡] and Yun-Sung Lee*[,†]

[†]School of Chemical Engineering, Chonnam National University, Gwang-ju 500-757, Republic of Korea

[‡]Department of Chemical Engineering, University of Waterloo, Waterloo, Ontario N2L 3G1, Canada

[§]Department of Material Science and Engineering, Seoul National University, 599 Gwanangno, Gwanak-gu, Seoul 151-742, South Korea

Supporting Information

**ABSTRACT:** Despite their high specific capacity, sodium layered oxides suffer from severe capacity fading when cycled at higher voltages. This key issue must be addressed in order to develop high-performance cathodes for sodium ion batteries (SIBs). Herein, we present a comprehensive study on the influence of Al doping of Mn sites on the structural and electrochemical properties of a P2–$Na_{0.5}Mn_{0.5-x}Al_xCo_{0.5}O_2$ ($x$ = 0, 0.02, or 0.05) cathode for SIBs. Detailed structural, morphological, and electrochemical investigations were carried out using X-ray diffraction, cyclic voltammetry, and galvanostatic charge–discharge measurements, and some new insights are proposed. Rietveld refinement confirmed that Al doping caused $TMO_6$ octahedra (TM = transition metal) shrinkage, resulting in wider interlayer spacing. After optimizing the aluminum concentration, the cathode exhibited remarkable electrochemical performance, with better stability and improved rate performance. Electrochemical impedance spectroscopy (EIS) measurements were performed at various states of charge to probe the surface and bulk effects of Al doping. The material presented here exhibits exceptional stability over 100 cycles within a 1.5–4.3 V window and outperforms several other Mn–Co-based cathodes for SIBs. This study presents a facile method for designing structurally stable cathodes for SIBs.

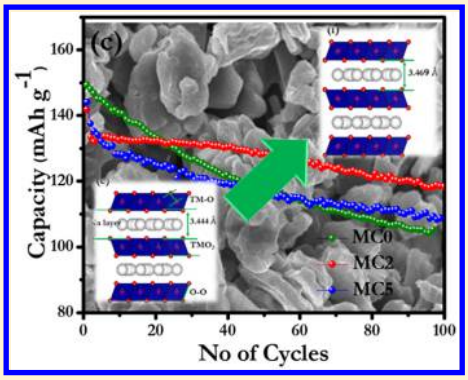


Rechargeable lithium ion batteries (LIBs) are used in a wide range of consumer electronics. Higher-energy-density LIBs are already dominating the current automobile market including hybrid electric vehicles (HEVs), plug in hybrid electric vehicles (PHEVs), and full electric vehicles (FEVs). However, geographical constraints impose high costs on lithium and thus LIBs.[1,2] Sodium ion batteries (SIBs) are found to be the future of energy storage as they have the wide potential to complement the LIBs to a greater extent. In addition, SIBs are low-cost and highly safe, and sodium resources are widely available on the earth's crust (sodium is the fourth-most abundant element on the earth's crust).[1] The working principle of SIBs is similar to that of LIBs and involves the migration of cations/anions across a separator toward electrodes to realize voltage-driven electrochemical reactions.[2] Gravimetric energy density is not a serious issue for the large-scale energy storage systems required for smart grids and the storage of intermittent energy sources like solar and wind power; thus, SIBs are a natural choice for these applications.[3] Several reported SIB anode materials have exhibited capacities of around 400 mAh $g^{-1}$ and voltage ranges of 0.1–0.6 V. Thus, researchers must focus on developing new cathodes to have the greatest chance of improving the operating voltage of SIBs.[3] Although sodium and lithium metals exhibit similar physical and chemical properties, the larger radii of the $Na^+$ ion remains a hurdle in developing structurally stable cathode materials for SIBs.

Recently, numerous host materials with reversible sodium storage behavior have been widely reported, including layered oxides,[4,48,49] polyanion materials,[5] and Prussian blue[6] analogues. Among these materials, layered transition metal oxides (TMOs) have been significantly studied due to their rich diversity of structure and ease of synthesis. Additionally, they can accommodate single, binary, and ternary TM ions that undergo redox reactions during charging and discharging, resulting in high discharge capacities.[7] These layered oxides have a common structure that consists of sheets of edge-sharing $TMO_6$ octahedra.[8] Polymorphisms appear as a result of variations in the stacking of these layers along the $c$-axis.[9] Layered oxides are differentiated into two different forms, prismatic (P) and octahedral (O), based on the coordination of the Na ion in the layered structure. They can be further classified into more specific types, such as P2, P3, and O3, depending on the number of TM layers in the unit cell.[9] These materials are very sensitive toward calcination, Na-ion

**Received:** August 1, 2017
**Accepted:** September 15, 2017
**Published:** September 15, 2017




DOI: 10.1021/acs.jpclett.7b02012
J. Phys. Chem. Lett. 2017, 8, 5021–5030

**Scheme 1. Procedure for Synthesis of MC Samples Using a Sol−Gel Method**

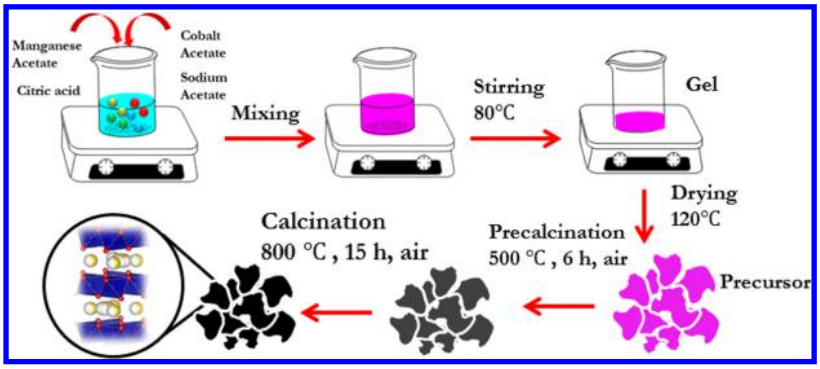


stoichiometry, and their synthesis parameters.[10,11] In terms of cyclic stability and rate performance, P2-type materials were found to be better than O3-type materials.[12] This is due to the larger tunnel for alkali ion diffusion in P2-type layered oxides, resulting in improved electrochemical performance compared with O3-type layered oxides.[7] Despite these good structural properties, the cyclic stability and energy density of P2-type materials is severely affected by the P2−O2 phase transition that occurs during the extensive deintercalation of Na ions from layered oxides, which results in the inferior rate capability of P2-type cathodes in comparison to O3-type layered oxides.[13]

Hence, designing advanced electrode materials with an optimized composition is essential for obtaining highly economic, safe, and long-life cathodes with high energy densities for SIBs. Using manganese-based cathodes provides low-cost, safe, and sustainable batteries due to the high abundance and low toxicity of manganese.[2] Many manganese-based P2 cathodes with good electrochemical properties have been reported over the past few years.[4] The drawback of $Mn^{3+}$-based cathodes lies in their capacity fading, which arises from Jahn−Teller deformation caused by the $Mn^{3+}$ ions and results in the appearance of multiple voltage steps in the discharge curve.[14] Despite these drawbacks, many researchers have tried to modify $Mn^{3+}$-based cathodes by introducing foreign metals into their structure. Yabuchi et al. reported a P2−$NaFe_{0.5}Mn_{0.5}O_2$ cathode that delivered 190 mAh $g^{-1}$ at 12 mA $g^{-1}$, but its stability was not impressive.[15] Wang et al. synthesized P2−$Na_{2/3}Mn_yCo_{1-x}O_2$ with varying composition using a solid-state method, but it suffered from capacity fading.[16] P2−$Na_{0.5}[Ni_{0.23}Fe_{0.13}Mn_{0.63}]O_2$ exhibited a high capacity, delivering 200 mAh $g^{-1}$ at a rate of 15 mA $g^{-1}$, but with inferior rate performance.[9] Li et al.[17] reported P2−$Na_{7/9}Cu_{2/9}Fe_{1/9}Mn_{2/3}O_2$ as a promising air-stable cathode with $Cu^{2+}/Cu^{3+}$ redox activity, but it could deliver only 60 mAh $g^{-1}$ at a 1C rate over 150 cycles. Larger Na ions create more stress accompanied by a large volume change during charge/discharge, which causes severe capacity fading in SIB cathodes.[18] Optimizing the composition of SIB cathodes can greatly improve their electrochemical performance for the practical realization of ambient-temperature SIBs.[19]

Various design strategies have been adopted to optimize the composition of cathodes, including (i) morphological variation,[20] (ii) surface coating with metal oxides,[21] and (iii) introducing an inactive dopant into the lattice.[22] Substituting cheap and lightweight dopants with similar radii to Mn, such as Mg, Al, Ni, Co, and Cr, into the cathode structure changes the local atomic arrangements, which was found to improve its electronic conductivity and stability.[23] Many attempts have been made to prevent the sodium-driven phase transition in P2-type layered oxides. Yuan et al. synthesized P2−$Na_{0.67}Mn_{0.65}Ni_{0.15}Co_{0.2}O_2$ using a sol−gel method. They partially replaced the $Co^{3+}$ ions with $Al^{3+}$ ions, resulting in improved cycling stability.[4] Billaud et al. synthesized an earth-abundant P2−$Na_{0.67}Mn_{1-x}Mg_xO_2$, where 5% Mg content smoothed the structure; increasing the Mg content improved the stability at the expense of a little capacity and improved the cathode cyclability.[24] Substituting Zn into P2-type $Na_{0.67}Ni_{0.33}Mn_{0.67}O_2$ prevented the $Na^+$/vacancy ordering and improved its average voltage and capacity retention.[22] Clemet et al. studied in detail the effects of Mg doping P2 layered structures and found that it reduces the content of Jahn−Teller-active $Mn^{3+}$, delays the high-voltage phase transition, and thereby increases the capacity retention and rate capability of these materials.[25] Mg substitution suppressed the high-voltage P2−O2 phase transition of P2−$Na_{0.67}Mn_{0.67}Ni_{0.33}O_2$.[26,13,27]

Our present work is motivated by previous SIB reports that suggest the positive role that metal-ion doping can play in improving the capacity, electrochemical stability, and rate capability of SIB cathodes. We synthesized a series of Al-doped $Na_{0.5}Mn_{0.5-x}Al_xCo_{0.5}O_2$ ($x$ = 0, 0.02, or 0.05) materials using a simple sol−gel method with citric acid as a chelating agent. The positive effects of Al doping on the structural and electrochemical properties of this Na−Mn−Co-based compound are analyzed in detail. Aluminum is abundant, inexpensive, and lightweight, with a similar radius (0.53 Å) as $Mn^{3+}$ (0.66 Å), thus making the substitution easier. Correspondingly, the Al−O bond is stronger than the Mn−O bond, which strengthens the cathode structure over long cycles.[28] Rietveld refinement measurements confirmed that Al-doping causes shrinkage of the $TMO_6$ octahedra, with enlarged $d$ spacing and a wider Na-ion diffusion layer, resulting in very stable cycling performance at higher voltages. The morphological features of Al-doped $Na_{0.5}Mn_{0.5-x}Al_xCo_{0.5}O_2$ were analyzed using scanning electron microscopy (SEM) and X-ray photoelectron spectroscopy (XPS), and its electrochemical properties were analyzed using cyclic voltammetry (CV), galvanostatic charge−discharge, and electrochemical impedance spectroscopy (EIS) measurements. All samples could be reversibly charged and discharged within an extended voltage range of 1.5−4.3 V. We found that doping 0.02 mol of $Al^{3+}$ was sufficient to produce good structural stability, with 83% capacity retention over prolonged cycling. There are no other reports solely on substituting aluminum for redox-active Mn for SIBs. Our work is significant due to the stabilization effect found upon replacing Mn in the lattice with Al, and our results suggest that this is a facile way of designing improved cathode materials for room-temperature SIBs.



DOI: 10.1021/acs.jpclett.7b02012
J. Phys. Chem. Lett. 2017, 8, 5021−5030

The $Na_{0.5}Mn_{0.5-x}Al_xCo_{0.5}O_2$ ($x$ = 0, 0.02, or 0.05) samples were synthesized using a citric-acid-assisted sol−gel method, as shown in Scheme 1. Choosing an appropriate amount of sodium precursor is the most important part of this cathode synthesis as this determines the final cathode structure. An excess amount of sodium acetate (5%) was added during synthesis in order to balance the loss of sodium during the high-temperature annealing process. The chemical composition of all samples was determined using ICP-AES measurements, and the resulting values are given in Table 1. The obtained values are similar to calculated values with only slight deviations. Hereafter, the $Na_{0.5}Mn_{0.5-x}Al_xCo_{0.5}O_2$ samples are denoted as MC0, MC2, and MC5 for $x$ = 0, 0.02, and 0.05, respectively. The cathode material has a lower sodium content with a defective TM ratio of 0.5 instead of 1, which results in the phase stabilization of the material. The results of the XRD and Rietveld analyses are presented in Figure 1. The XRD peaks indicate a P2 structure with a $P63/mmc$ (no. 194) space group, and there is no sign of any impurity phases after doping with Al atoms. Rietveld refinement was carried out to better understand the effects of Al doping, and the lattice parameter values for all samples are presented in Table 2. The lattice parameters for the pristine sample are $a$ = 2.821 Å and $c$ = 11.212 Å, which are identical to the reported values.[29] The $a$ value remains constant upon increasing the amount of Al, while the $c$ value decreases. This is due to shortening of the Al−O bonds after substitution.[4] The refinement results, along with the atomic occupancies, for each sample are shown in Tables 3−6. The $d$ spacing is 3.444 Å for MC0 and gradually increases to 3.469 and 3.481 Å for MC2 and MC5, respectively. The TM−O bond concurrently decreases with increasing aluminum content: 1.955, 1.948, and 1.940 Å for MC0, MC2, and MC5, respectively. The amount of Na used in the synthesis matches with the refined value of 0.5 mol for all samples. The majority of Na ions prefer a Na (2) site as it is electrostatically more favorable than the other Na sites.[30]

**Table 1. Results of ICP-AES Analysis for the As-Prepared Samples**

| | Na | Mn | Al | Co |
|---|---|---|---|---|
| | Ratios Determined by ICP Analysis | | | |
| MC0 | 0.503 | 0.508 | 0 | 0.491 |
| MC2 | 0.510 | 0.496 | 0.019 | 0.483 |
| MC5 | 0.505 | 0.467 | 0.041 | 0.490 |
| | Calculated Ratios | | | |
| MC0 | 0.5 | 0.5 | 0 | 0.5 |
| MC2 | 0.5 | 0.48 | 0.02 | 0.5 |
| MC5 | 0.5 | 0.45 | 0.05 | 0.5 |

The crystal structures of the three samples were constructed using the data obtained from the Rietveld analysis, and the corresponding images are presented in Figure 1e−g. In general, the layered oxides consist of a sodium layer and a $TMO_6$ octahedron layer arranged alternatively to form a "sandwich"-type structure along the $c$ axis.[7] In the case of SIBs, the wide interlayer spacing is necessary for facile Na-ion insertion.[31] This structural data provides useful information about the local environment, which explains the higher stability of the $Al^{3+}$-doped samples. The TM−O and O−O bond lengths and the slab thickness of the $TMO_6$ octahedron all decrease as a result of the decreased Al−O bond length,[28] which results in improved structural stability. The increased $d$ spacing of the Al-doped samples arises from the contraction of the $TMO_6$ octahedra without affecting the number of TM layers. The $TMO_6$ volume shrinkage originates from the reduced TM−O and O−O bond lengths. The larger $d$ spacing decreases the activation barrier for Na-ion diffusion, resulting in a high rate capability for the cathode, with improved diffusion kinetics during (de)sodiation.[32] P2-type layered oxides have two different prismatic sites for Na-ion occupancy: Na (1) and Na (2). Na (1) sites share faces with $MO_6$ octahedra, whereas Na (2) sites share edges with $MO_6$ octahedra.[33] The distribution of Na ions in these sites depends on the electrostatic repulsion between $Na^+$ ions and the TM ions and in-plane $Na^+$−$Na^+$ interactions. $Na^+$/vacancy ordering is also present in these P2 structures, as reported by various groups.[30]

XPS was performed to determine the oxidation states of the TMs present in the cathodes. Figure 2 shows the Mn, Co, and Al XPS spectra for MC0, MC2, and MC5. The Mn 2p spectra show two major peaks corresponding to Mn $2p_{3/2}$ and Mn $2p_{1/2}$, which can be deconvoluted into four peaks. The two peaks located at 643 and 654 eV correspond to $Mn^{4+}$, while the peaks located at 642 and 653 eV correspond to $Mn^{3+}$, which is consistent with previously reported values.[34] The two major cobalt peaks present at 779.5 and 794.5 eV correspond to Co $2p_{3/2}$ and Co $2p_{1/2}$, respectively.[34] This indicates a Co valence state of +3.[34] The MC2 and MC5 spectra exhibit a peak located at 74.3 eV, which corresponds to Al 2p.[35] The $Al^{3+}$ ions do not take part in the electrochemical processes of the cathode and, thus, make no contribution to its capacity. Moreover, the peak positions for all elements did not vary between the three samples, which confirms that Mn, Co, and Al exist in the same oxidation state in the three different cathodes. All samples were analyzed using FESEM (Figure 3) in order to characterize the influence of Al doping on the cathode morphology. All samples look alike, with little variation in size and shape; this is attributed to the minimal amount of aluminum doping. The average particle size is about 3−5 $\mu$m in length, with a thickness of 1 $\mu$m. Figure 3a shows a high-magnification FESEM image of MC2, and Figure 3b shows a TEM image of a single MC2 particle with an irregular Flake-like morphology. An SAED pattern (Figure 3c) was recorded during TEM analysis to further probe the MC2 structure. This pattern clearly shows the (001) zone axis of the single crystallite from which the interplanar distance was calculated along the (100) zone to be 2.48 Å. Figure 3d−i shows Na, Mn, Co, Al, and O elemental maps of MC2, with all elements uniformly distributed over the entire particle.

The MC0, MC2, and MC5 cathodes were characterized electrochemically using CV and galvanostatic charge/discharge measurements. Figure 4a shows CV curves of the three samples in a voltage range of 1.5−4.3 V recorded at a scan rate of 0.5 mV $s^{-1}$. All cells exhibited an open-circuit potential of 2.8 V.[10] The appearance of multiple redox peaks in the CV curves can be ascribed to the participation of different metal ions in the electrochemical charge/discharge process. The redox peak below 2.0 V is attributed to the $Mn^{4+}/Mn^{3+}$ redox couple, while the peaks above 3.0 V correspond to the $Co^{4+}/Co^{3+}$ redox couple.[34] In line with other reports, Mn does not contribute to the capacity when the cutoff voltage is restricted to 2.0 V. However, when the cell is discharged to 1.5 V, $Mn^{4+}$ is activated and contributes a reversible capacity, as evident from the CV curves.[36] The peaks appear to be the same for all three samples, irrespective of the small amount of aluminum doping in MC2



DOI: 10.1021/acs.jpclett.7b02012
J. Phys. Chem. Lett. 2017, 8, 5021−5030

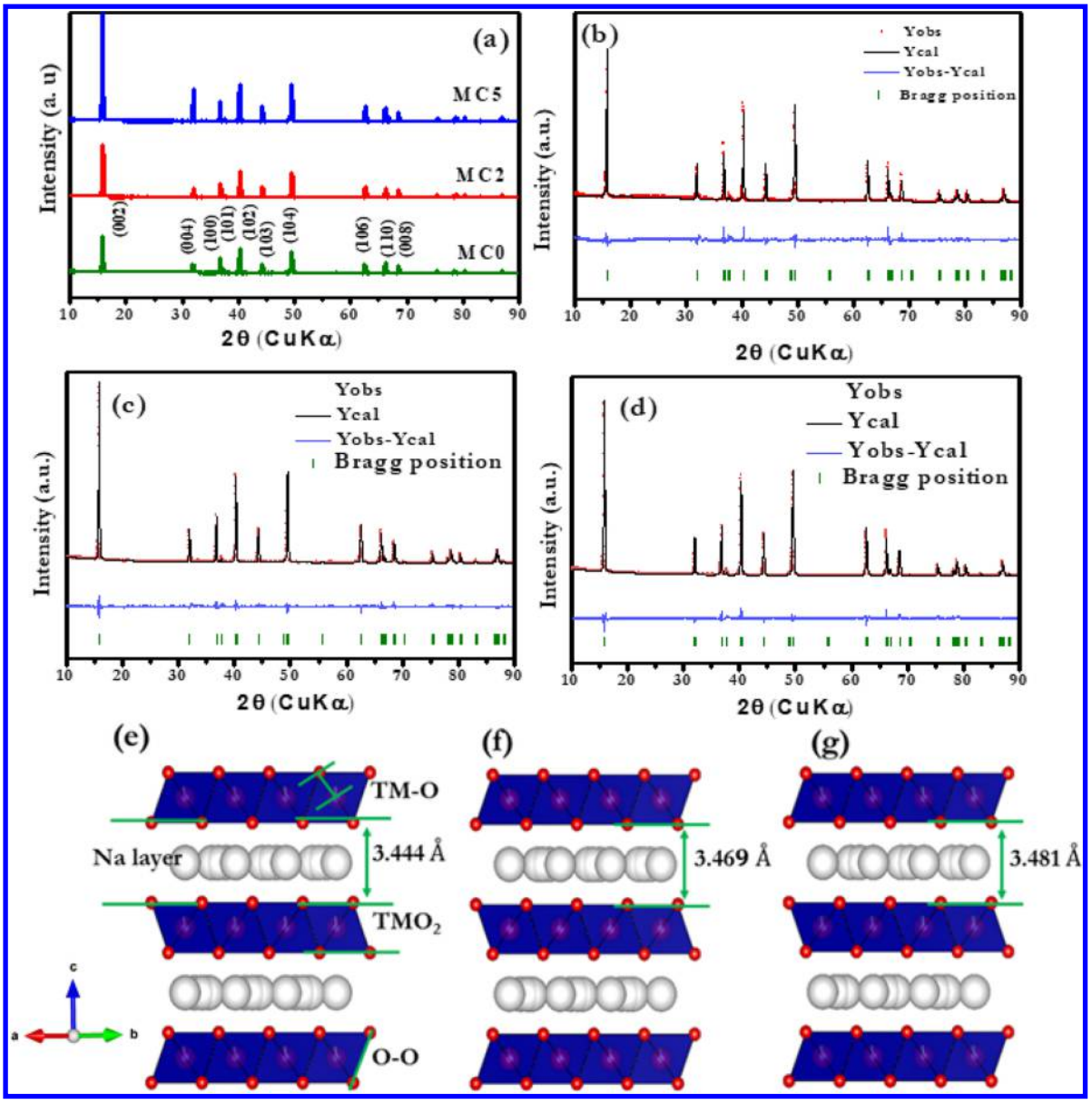


**Figure 1.** (a) XRD patterns for MC0, MC2, and MC5. (b–d) Rietveld refinement results for MC0 (b), MC2 (c), and MC5 (d) with their observed and calculated values. (e–g) Refined structure of each material. Gray, red, and pink atoms correspond to Na, O, and TM (TM = Mn, Al, Co): (e) MC0, (f) MC2, and (g) MC5.

**Table 2. Refined Crystallographic Parameters for the As-Prepared Samples**

| samples | *a*/Å | *c*/Å | cell volume/Å$^3$ | fitting factors $R_p$ (%) |
|---|---|---|---|---|
| MC0 | 2.82172(16) | 11.21243 (79) | 77.314(8) | 9.84 |
| MC2 | 2.82270(13) | 11.20426 (61) | 77.312(7) | 9.09 |
| MC5 | 2.82142(11) | 11.17981 (51) | 77.073(5) | 8.35 |

**Table 3. Refined Crystal Site and Atomic Occupancies of MC0**

| atom | site | *x* | *y* | *z* | occ. |
|---|---|---|---|---|---|
| Na1 | 12j | 0.52900 | 0.19000 | 0.25000 | 0.101 |
| Na2 | 2b | 0.00000 | 0.00000 | 0.25000 | 0.447 |
| Mn | 2a | 0.00000 | 0.00000 | 0.00000 | 0.480 |
| Co | 2a | 0.00000 | 0.00000 | 0.00000 | 0.480 |
| O | 4f | 0.33333 | 0.66667 | 0.09640 | 1.000 |

**Table 4. Refined Crystal Site and Atomic Occupancies of MC2**

| atom | site | *x* | *y* | *z* | occ. |
|---|---|---|---|---|---|
| Na1 | 12j | 0.55900 | 0.21300 | 0.25000 | 0.086 |
| Na2 | 2b | 0.00000 | 0.00000 | 0.25000 | 0.404 |
| Mn | 2a | 0.00000 | 0.00000 | 0.00000 | 0.497 |
| Co | 2a | 0.00000 | 0.00000 | 0.00000 | 0.484 |
| Al | 2a | 0.00000 | 0.00000 | 0.00000 | 0.019 |
| O | 4f | 0.33333 | 0.66667 | 0.09520 | 1.000 |

and MC5. This is attributed to the chemical inertness of the dopant, which means its participation in the electrochemical charge/discharge process is minimal.[37]

Figure 4b shows the initial charge/discharge curves for all three samples in a voltage range of 1.5–4.3 V at a current rate of 85 mA g$^{-1}$ (1C = 136 mAh g$^{-1}$). The well-balanced atomic stoichiometry of Mn and Co makes the cathodes more stable



DOI: 10.1021/acs.jpclett.7b02012
J. Phys. Chem. Lett. 2017, 8, 5021–5030

**Table 5. Refined Crystal Site and Atomic Occupancies of MC5**

| atom | site | *x* | *y* | *z* | occ. |
|---|---|---|---|---|---|
| Na1 | 12j | 0.55100 | 0.26400 | 0.25000 | 0.092 |
| Na2 | 2b | 0.00000 | 0.00000 | 0.25000 | 0.430 |
| Mn | 2a | 0.00000 | 0.00000 | 0.00000 | 0.458 |
| Co | 2a | 0.00000 | 0.00000 | 0.00000 | 0.482 |
| Al | 2a | 0.00000 | 0.00000 | 0.00000 | 0.035 |
| O | 4f | 0.33333 | 0.66667 | 0.09430 | 1.000 |

**Table 6. Interatomic Distances, Slab Thicknesses, and *d* Spacings of the Na Layer for All Samples**

| | MC0 | MC2 | MC5 |
|---|---|---|---|
| TM−O (Å) | 1.955 | 1.948 | 1.940 |
| $TMO_2$ (Å) | 2.162 | 2.133 | 2.109 |
| O−O (Å) | 2.707 | 2.685 | 2.664 |
| Na1−O (Å) | 2.153 | 2.193 | 2.280 |
| Na2−O (Å) | 2.371 | 2.380 | 2.384 |
| *d* spacing (Å) | 3.444 | 3.469 | 3.481 |

over the entire 1.5−4.3 V voltage range. The polarization observed in the initial charge/discharge curve is attributed to several factors including electrolyte degradation at higher voltages, structural changes, and the presence of impurities; this causes capacity fading over prolonged cycling.[9] The charge/discharge curves display a smooth voltage plateau without any step-like voltage features, which is a common feature of mixed binary TMOs.[24] In a previous study, we focused on the suppression of stepwise voltage plateaus using structural doping and metal oxide coating.[13] Herein, we focused on the impact of foreign elements replacing Mn ions in the MC0 structure. Two voltage plateaus appear in the charge/discharge curve of MC0 at 3.9 and 1.8 V, corresponding to the redox reactions of $CO^{2+}/Co^{3+}$ and $Mn^{4+}/Mn^{3+}$, respectively.[29] MC0 delivers an initial capacity of 149 mAh $g^{-1}$ at 85 mA $g^{-1}$, whereas the initial capacity of the aluminum-doped samples is considerably reduced to 141 and 143 mAh $g^{-1}$ for MC2 and MC5, respectively. This is attributed to the replacement of redox-active Mn with electrochemically inactive aluminum ions.[38] However, the $Al^{3+}$-doped samples exhibit a higher Coulombic efficiency than the undoped sample; this indicates that MC2 and MC5 exhibit more reversible charge/discharge than MC0. The Coulombic efficiency of aluminum-doped samples remained around 97% except for the first few cycles, indicating the existence of irreversible decomposition of electrolyte in the initial few cycles. The separation between the charge/discharge curves is greater for MC0, with a visible voltage plateau. Doping in 0.02 mol of $Al^{3+}$ decreases the separation and increases the slope of the voltage plateau, which is attributed to the improved structural stability and wider interlayer spacing as evident from the XRD analysis. This indicates a reduced cyclic polarization in the cathode along with improved battery performance.[28] Figure 4c shows the cyclic stability of MC0, MC2, and MC5 over 100 cycles at a constant current rate of 85 mA $g^{-1}$. Initially, MC0 exhibits the highest capacity of 149 mAh $g^{-1}$, which is higher than that of many reported P2 layered cathode materials. However, MC0 undergoes severe capacity fading and only maintains 70% of its initial capacity after 100 cycles. There are several potential reasons for this capacity fading. Structural transition at higher voltages is the primary cause of capacity fading in many P-type layered oxides and originates from greater repulsion between the oxygen layers when a significant number of Na ions are deeply extracted from the cathode structure.[39] Considering the arrangements of atoms, the structure of P- and O-type cathodes can be easily explained. The stacking patterns of P2-type and O2-type materials are AABB and ABCB, respectively.[8,10] Hence, the phase transition from P- to O-type can occur easily by simple gliding of the oxygen layers without breaking TM−O

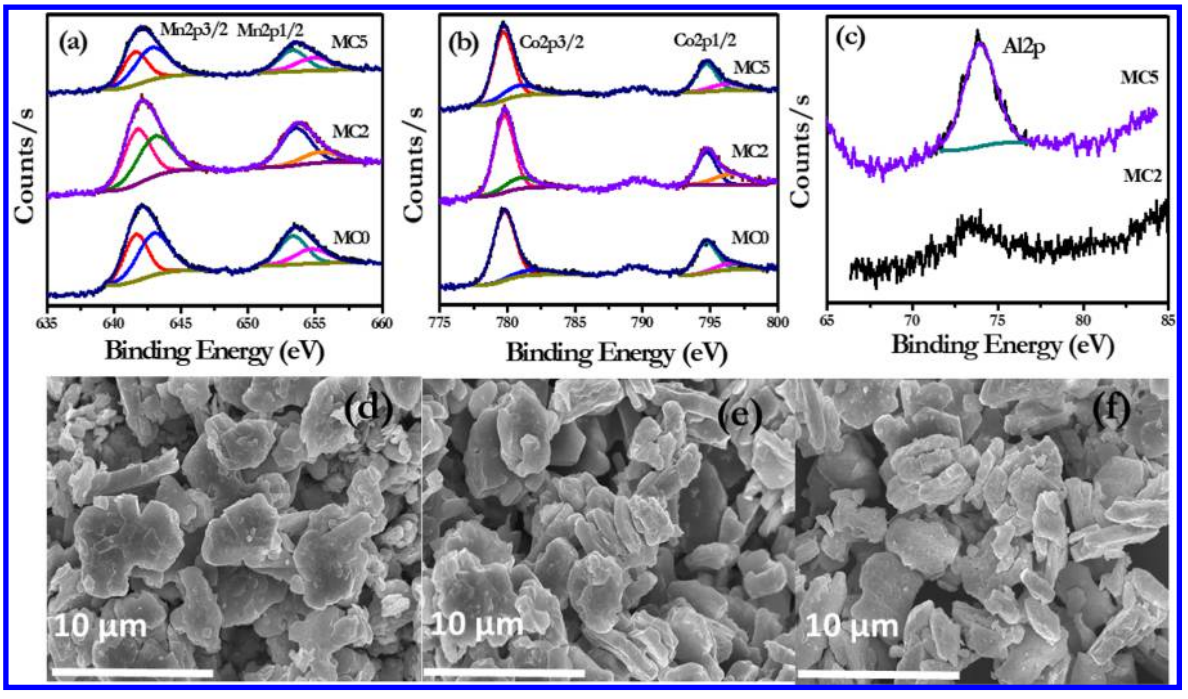


**Figure 2.** XPS Spectra and peak fittings for the different elements in the powder samples: (a) Mn, (b) Co, and (c) Al. SEM images of the samples: (d) MC0, (e) MC2, and (f) MC5.



DOI: 10.1021/acs.jpclett.7b02012
J. Phys. Chem. Lett. 2017, 8, 5021−5030

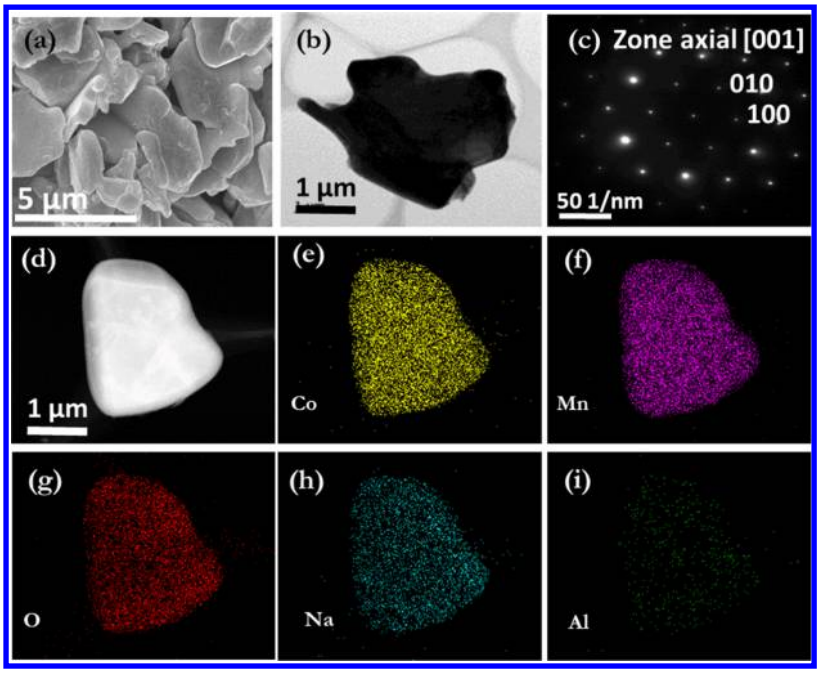


**Figure 3.** High-magnification FESEM (a) and TEM (b) images, SAED pattern (c), and elemental maps (d–i) of MC2.

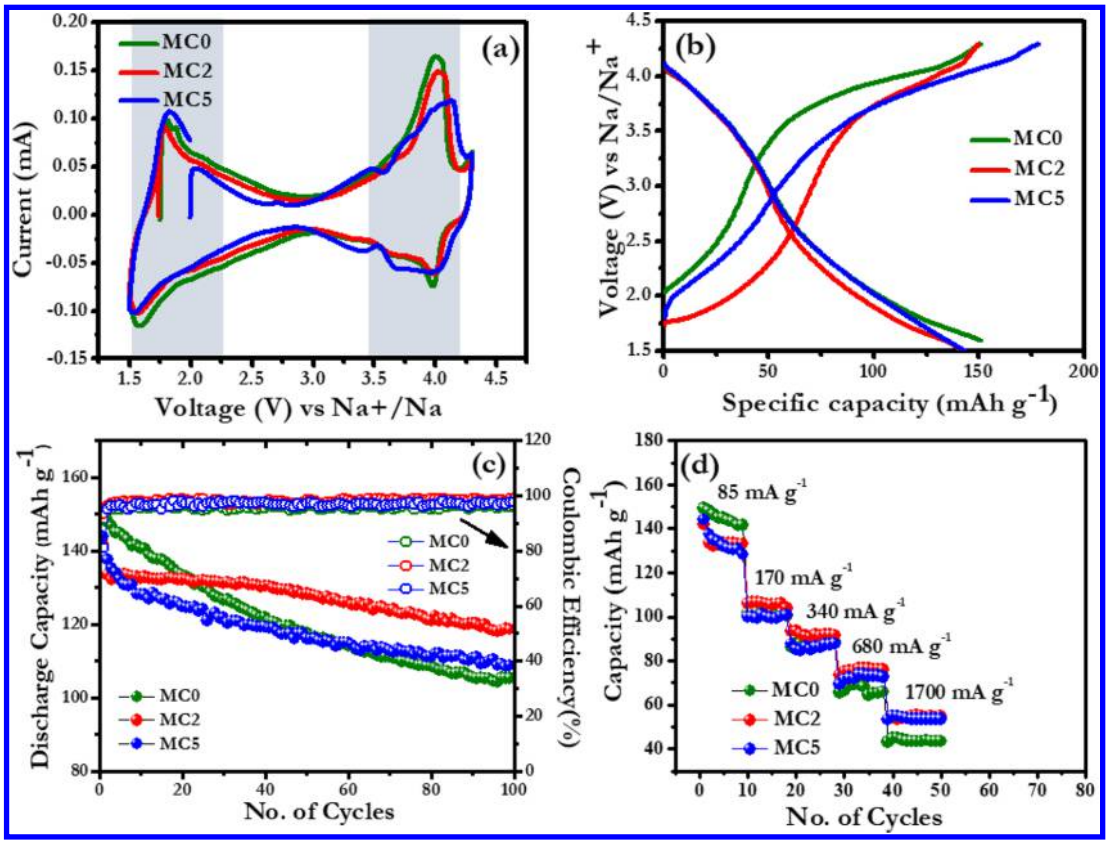


**Figure 4.** (a) CV curves for the three MC0, MC2, and MC5 samples recorded at a scan rate of 0.5 mV $s^{-1}$ in a voltage range of 1.5–4.3 V. (b) Galvanostatic charge/discharge curves for MC0, MC2, and MC5 recorded in a voltage range of 1.5–4.3 V at a current rate of 85 mA $g^{-1}$(1C = 134 mA $g^{-1}$). (c) Cyclic stability of MC0, MC2, and MC5 over 100 cycles at a 0.5C rate in a 1.5–4.3 V range. (d) Rate performance of the three MC0, MC2, and MC5 samples at current rates of 85, 170, 340, 680, and 1700 mA $g^{-1}$ between 1.5 and 4.3 V.

bonds.[8] Beyond this structural transition, the capacity fading in the initial few cycles may be caused by catalytic decomposition of the Na-based electrolyte at higher voltages.[40,41] Hence, restricting the cutoff voltage to around 4 V could be a good way to minimize the capacity fading at the expense of lower capacity. Similarly, manganese-based cathodes suffer from $Mn^{2+}$ dissolution at lower voltages due to Jahn–Teller distortion.[14] The $Mn^{3+/4+}$ redox couple is primarily electrochemically active



DOI: 10.1021/acs.jpclett.7b02012
J. Phys. Chem. Lett. 2017, 8, 5021–5030

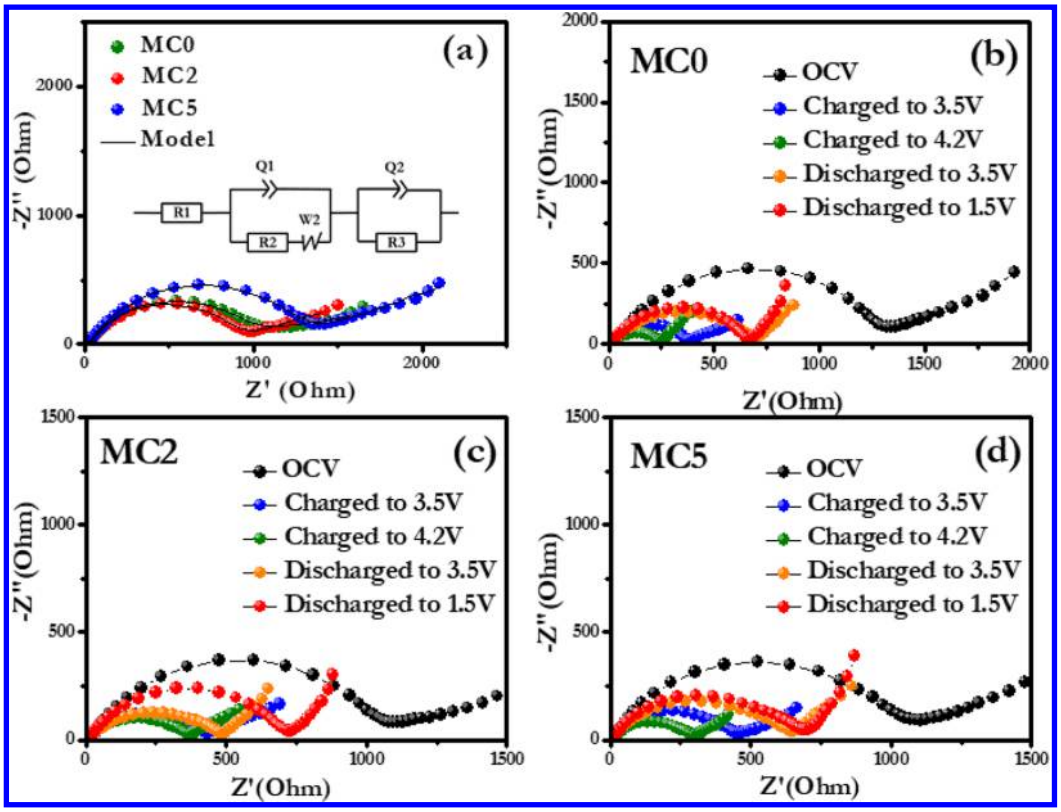


**Figure 5.** (a) Nyquist plots for MC0, MC2, and MC5. The inset shows the equivalent circuit for this system. (b–d) Nyquist plots measured at various equilibrium potentials for MC0, MC2, and MC5.

below 2.0 V. The MC0, MC2, and MC5 CV curves exhibit clear redox peaks below 2.0 V, which are attributed to the participation of Mn redox couples. Electrolyte decomposition and the formation of an SEI (solid–electrolyte interface) layer during the initial cycles cause irreversible capacity loss, which is a common character of high-voltage layered oxides. This reduces the participation of active material in the electrochemical process. Despite this initial capacity loss, it is clear that the aluminum-doped samples exhibit better structural stability than the pristine MC0 material. MC2 retains 83% of its capacity after 100 cycles, which is 12 percentage points higher than the MC0 capacity retention. This is attributed to a decrease in Jahn–Teller distortions upon replacing $Mn^{3+}$ with $Al^{3+}$ as this decreases the average $Mn^{3+}$ concentration, thereby improving the capacity retention.[38] The reduced Al–O bond length also creates a wider diffusion channel for $Na^+$ ions to diffuse smoothly without significant distortion of the layered structure. Upon increasing the Al doping to 0.05 mol (MC5), the performance decreases. This may be caused by greater $Al^{3+}$ doping in octahedral positions, which would result in lattice dislocation by occupying the Na diffusion pathway.[28] Thus, a moderate amount of aluminum doping is necessary for improved capacity retention, as shown in Figure 4.

To further probe the rate performance, all samples were charged/discharged in a voltage range of 1.5–4.3 V at different current densities, as shown in Figure 4d. The capacity gradually decreases with increasing current density due to the diffusion-controlled kinetics of the cathode materials.[28] MC0 displays capacities of 149, 101, 86, 65, and 43 mAh $g^{-1}$ at current rates of 85, 170, 340, 680, and 1700 mA $g^{-1}$, respectively. MC2 exhibits the highest rate capability, with capacities of 141, 106, 93, 73, and 53 mAh $g^{-1}$ at 85, 170, 340, 680, and 1700 mA $g^{-1}$, respectively, whereas MC5 exhibits capacities of 143, 100, 87, 69, and 53 mAh $g^{-1}$ at 85, 170, 340, 680, and 1700 mA $g^{-1}$, respectively. It can be seen that MC2 and MC5 exhibit superior rate capability compared with MC0. At lower current rates, the effect of aluminum doping is not obvious. However, as the current rate is increased, the aluminum-doped samples exhibit increasingly improved stability. This can be explained as follows. The electrochemical inactivity of $Al^{3+}$ is the reason for the low capacity at 85 mAh $g^{-1}$. However, the rate performance is dominated by the structural stability of the Al-doped samples, as confirmed by the XRD measurements. The strength of the Al–O (512 kJ $mol^{-1}$) bond compared with Mn–O (402 kJ $mol^{-1}$) prevents expansion and contraction of the layers during repeated insertion and deinsertion of $Na^+$ ions. The lower electronegativity of Al also increases the ionic bonding strength during cycling.[42,43] From our results, we conclude that doping an optimum amount of $Al^{3+}$ is vital for improving cathode performance. Moreover, the enlarged *d* spacing arising from Al doping is the origin of the high rate performance of MC2, which agrees well with the Rietveld refinement results. MC2 outperforms several reported P2-type layered oxides. For example, Hasa et al.[9] studied $Na_{0.5}Ni_{0.23}Fe_{0.13}Mn_{0.63}O_2$ as a high-capacity cathode for SIBs, but its rate performance was limited to 60 mAh $g^{-1}$ at 5C (715 mA $g^{-1}$). Liu et al.[44] reported P2–$Na_{0.6}Ni_{0.2}Co_{0.2}Mn_{0.5}Ti_{0.1}O_2$ with a capacity of 70 mAh $g^{-1}$ at a 5C rate. Hemalatha et al.[14] incorporated Ni and Mg into a P2–$Na_{0.67}MnO_2$ cathode in place of Jahn–Teller-active $Mn^{3+}$ ions, and this improved its electrochemical performance, though it could only deliver a capacity of 70 mAh $g^{-1}$ at 1C. P2–$Na_{0.6}Mn_{0.5}Fe_{0.5}O2$[15] has been reported as an earth-abundant cathode material with a highest-ever-reported capacity of 190 mAh $g^{-1}$ in a voltage


DOI: 10.1021/acs.jpclett.7b02012
J. Phys. Chem. Lett. 2017, 8, 5021–5030

range of 1.5−4.2 V; however, it could only deliver around 60 mAh $g^{-1}$ at a 4C rate (1040 mA $g^{-1}$), which is comparatively less than that reported here. Yuan et al.[4] developed P2−$Na_{0.67}Mn_{0.65}Co_{0.2}Ni_{0.15}O_2$ microflakes as a highly stable cathode material by partial substitution of $Al^{3+}$ ions in place of $Co^{3+}$ ions. The effects of aluminum doping in layered structures have been studied in several layered oxides. The higher strength of Al−O bonds could suppress the expansion and contraction of the interlayers in wider voltage windows. Al doping is thought to improve the stability of the cathode at higher voltages, as predicted by the theoretical calculations of Ceder et al.[45]

To understand the effect of aluminum doping on the kinetic performance of these electrodes, EIS studies were carried out, and the corresponding Nyquist plots are presented in Figure 5a. The inset in Figure 5a shows the corresponding equivalent circuit. Almost all samples exhibit same behavior, with a semicircle in the high-frequency region followed by a straight line in the low-frequency region. These measurements were carried out by applying a 10 mV AC potential in a frequency range of 1 MHz to 10 mHz after the first discharge. At first glance, the Nyquist plots indicate the dominance of charge-transfer and diffusion-controlled processes in the overall electrochemical reaction. In all curves, the high-frequency semicircle denotes the charge-transfer resistance and the sloping line in the low-frequency region denotes the Warburg impedance, which is mainly controlled by the diffusion of sodium ions in the bulk of the electrodes.[34] The MC2 semicircle is smaller than those for MC0 and MC5, which shows that MC2 has the lowest charge-transfer resistance and, thus, 0.02 mol of aluminum is sufficient to provide improved electrochemical performance in SIB cathodes.

Impedance is a powerful tool for determining both the bulk and surface properties of electrodes.[46] To understand the surface effects of aluminum doping, impedance measurements were conducted at different states of charge and discharge (Figure 5b−d) using the same measurement parameters described above. Before measurement, the cells were subjected to several charge/discharge cycles to activate and stabilize the electrodes. The impedance was measured during charge at 2.8, 3.5, and 4.2 V and during discharge at 3.5 and 1.5 V. The impedance spectra of these types of compounds cannot be treated quantitively.[37] However, qualitative analysis can clearly differentiate the surface and bulk effects over long-term operation. Changes in the high- to medium-frequency semicircle are indicative of electrode stability,[47] whereas the low-frequency response with respect to potential is indicative of the electronic and ionic conductivity of the cathode material during progressive (de)sodiation. All samples exhibit similar Nyquist plots at different states of charge, with small variations observable at higher voltages. The charge-transfer resistance of MC2 is smaller compared with those of MC0 and MC5 at a higher state of charge. This clearly indicates the better surface stability of MC2, even after the removal of Na ions at higher voltages. This stable structure can reversibly accommodate Na ions during discharge without significant capacity loss, which results in better capacity retention when cycled in a wider voltage window, as evident from the CV measurements. The impedance responses at 3.5 V during charging and discharging overlap most for the MC2 cathode. At deep discharging to 1.5 V, the impedance increases due to electrolyte decomposition and SEI layer formation (this film is partially insulating in nature).[19] Again, this highlights the significance of using an optimal amount of aluminum doping in layered structures. All of these results confirm the significance of aluminum doping in the bulk on the surface stabilization of high-voltage cathodes.

In summary, we have reported the synthesis of P2−$Na_{0.5}Mn_{0.48}Al_{0.02}Co_{0.5}O_2$ (MC2) as a novel cathode material for SIBs using a simple sol−gel method. Rietveld refinement confirmed the shrinking of $MeO_6$ octahedra upon Al doping, as a result of the reduced Al−O bond length, and a corresponding increase in the $d$ spacing of the Na diffusion layer. XPS measurements confirmed that aluminum doping does not change the valence state of the Mn and Co ions. These Al-doped microflakes exhibited a specific capacity of 141 mAh $g^{-1}$ in a voltage window of 1.5−4.3 V at a current density of 85 mAh $g^{-1}$. Although Al is chemically inactive, it improved the electrochemical performance of MC2, with 83% capacity retention over 100 cycles. This originates from the bulk- and surface-stabilization effects of aluminum doping, as confirmed by Rietveld and EIS analyses. This work will help in developing highly stable cathodes for large-scale energy storage applications in the future.

## EXPERIMENTAL METHODS

The layered oxide $Na_{0.5}Mn_{0.5}Co_{0.5}O_2$ (MC0) was prepared using a citric-acid-assisted sol−gel method, as outlined in Scheme 1. Stoichiometric amounts of sodium acetate ($CH_3COONa$, Sigma-Aldrich), manganese acetate tetrahydrate ($Mn(CH_3COO)_2{\cdot}4H_2O$, Sigma-Aldrich), and cobalt acetate tetrahydrate ($Co(CH_3COO)_2{\cdot}4H_2O$, Sigma-Aldrich) were dissolved separately in water (50% aqueous) and stirred separately for 30 min until the metal precursors were completely dissolved. This solution was added dropwise into a 60 wt % aqueous solution of citric acid. The final solution was stirred at 80 °C until a gel precursor formed. The gel precursor was kept at 120 °C overnight to obtain a powder precursor. The dried powder was heated at 500 °C for 6 h to decompose nitrate and eliminate water. The sample was then ground, pelletized, and heated at 800 °C for 15 h to obtain the final product. MC2 ($Na_{0.5}Mn_{0.48}Al_{0.02}Co_{0.5}O_2$) and MC5 ($Na_{0.5}Mn_{0.45}Al_{0.05}Co_{0.5}O_2$) samples were obtained using the same method with the addition of a corresponding amount of Al $(NO_3)_3{\cdot}6H_2O$ to replace the Mn acetate.

XRD patterns of the samples were obtained over a $2\theta$ range of 5−90° at a scanning rate of 2° $m^{-1}$ using Cu K$\alpha$ radiation. Rietveld analysis was performed to determine the structural parameters after metal-ion doping. The elemental composition of the samples was analyzed using inductively coupled plasma atomic energy spectroscopy (ICP-AES). The valence state of the elements was identified using XPS. The morphology and microstructure of the samples were analyzed using field emission scanning electron microscopy (FE-SEM), selected area electron diffraction (SAED), energy-dispersive spectroscopy (EDS), and high-resolution transmission electron microscopy (HRTEM).

The electrochemical performance of all samples was studied using CR2032 coin cells, which were assembled inside of a glovebox filled with ultrapure argon in which the $O_2$ and $H_2O$ levels were maintained below 1 ppm. The synthesized materials were used as cathodes, and Na metal was the anode; Whatman glass-fiber filter paper was used as a separator, and 1 M $NaClO_4$ in ethylene carbonate/diethyl carbonate (1:1) was used as the electrolyte. Each cathode consisted of 2.5 mg of the active material mixed with 0.5 mg of Ketjan black and 0.5 mg of Teflonized acetylene black (TAB). The obtained slurry with the assistance of ethanol was pressed on a stainless steel current


DOI: 10.1021/acs.jpclett.7b02012
J. Phys. Chem. Lett. 2017, 8, 5021−5030

collector and dried in a vacuum oven at 160 °C for 4 h before cell fabrication. Charge/discharge studies were performed in a voltage range of 1.5−4.3 V, with varying current rates of 85, 170, 340, 650, and 1700 mAh $g^{-1}$ using an Arbin BT-2000 battery test system. CV and impedance measurements were conducted using an electrochemical analyzer (SP-150, Biologic, France).

## ■ ASSOCIATED CONTENT

### Supporting Information

The Supporting Information is available free of charge on the ACS Publications website at DOI: 10.1021/acs.jpclett.7b02012.

Charge, discharge, and Coulombic efficiency plots, capacity retention vs cycle plots, and a comparison between reported P2-type cathodes and our work (PDF)

## ■ AUTHOR INFORMATION


### Corresponding Author

*E-mail: leeys@chonnam.ac.kr.

### ORCID

Hari Vignesh Ramasamy: 0000-0002-8241-2441

Kisuk Kang: 0000-0002-8696-1886

Zhongwei Chen: 0000-0003-3463-5509

Yun-Sung Lee: 0000-0002-6676-2871


### Notes

The authors declare no competing financial interest.

## ■ ACKNOWLEDGMENTS

This study was supported by the National Research Foundation of Korea (NRF) grant funded by the Korea government (Ministry of Science, ICT & Future Planning) (No. 2016R1A4A1012224).

## ■ REFERENCES


(1) Wang, L. P.; Yu, L.; Wang, X.; Srinivasan, M.; Xu, Z. J. Recent Developments in Electrode Materials for Sodium-Ion Batteries. *J. Mater. Chem. A* **2015**, *3*, 9353−9378.

(2) Ortiz Vitoriano, N.; Drewett, N.; Gonzalo, E.; Rojo, T. High Performance Manganese-Based Layered Oxide Cathodes: Overcoming the Challenges of Sodium Ion Batteries. *Energy Environ. Sci.* **2017**, *10*, 1051−1074.

(3) Dai, Z.; Mani, U.; Tan, H. T.; Yan, Q. Advanced Cathode Materials for Sodium-Ion Batteries: What Determines Our Choices? *Small Methods* **2017**, *1*, 1700098.

(4) Yuan, D.; He, W.; Pei, F.; Wu, F.; Wu, Y.; Qian, J.; Cao, Y.; Ai, X.; Yang, H. Synthesis and Electrochemical Behaviors of Layered {Na}0.67[{Mn}0.65Co0.2Ni0.15]{O}2 Microflakes as a Stable Cathode Material for Sodium-Ion Batteries. *J. Mater. Chem. A* **2013**, *1*, 3895−3899.

(5) Fang, J.; Wang, S.; Li, Z.; Chen, H.; Xia, L.; Ding, L.; Wang, H. Porous Na3V2(PO4)3@C Nanoparticles Enwrapped in Three-Dimensional Graphene for High Performance Sodium-Ion Batteries. *J. Mater. Chem. A* **2016**, *4*, 1180−1185.

(6) Fu, H.; Liu, C.; Zhang, C.; Ma, W.; Wang, K.; Li, Z.; Lu, X.; Cao, G. Enhanced Storage of Sodium Ions in Prussian Blue Cathode Material through Nickel Doping. *J. Mater. Chem. A* **2017**, *5*, 9604−9617.

(7) Han, M. H.; Gonzalo, E.; Singh, G.; Rojo, T. A Comprehensive Review of Sodium Layered Oxides: Powerful Cathodes for Na-Ion Batteries. *Energy Environ. Sci.* **2015**, *8*, 81−102.

(8) Chagas, L. G.; Buchholz, D.; Vaalma, C.; Wu, L.; Passerini, S. P-Type $Na_x$ $Ni_{0.22}$ $Co_{0.11}$ $Mn_{0.66}$ $O_2$ Materials: Linking Synthesis with Structure and Electrochemical Performance. *J. Mater. Chem. A* **2014**, *2*, 20263−20270.

(9) Hasa, I.; Buchholz, D.; Passerini, S.; Scrosati, B.; Hassoun, J. High Performance Na 0.5 [Ni 0.23 Fe 0.13 Mn 0.63 ]O 2 Cathode for Sodium-Ion Batteries. *Adv. Energy Mater.* **2014**, *4*, 1400083.

(10) Sathiya, M.; Hemalatha, K.; Ramesha, K.; Tarascon, J.-M.; Prakash, a. S. Synthesis, Structure, and Electrochemical Properties of the Layered Sodium Insertion Cathode Material: NaNi1/3Mn1/3Co1/3O2. *Chem. Mater.* **2012**, *24*, 1846−1853.

(11) Xie, M.; Luo, R.; Lu, J.; Chen, R.; Wu, F.; Wang, X.; Zhan, C.; Wu, H.; Albishri, H. M.; Al-Bogami, A. S.; et al. Synthesis-Microstructure-Performance Relationship of Layered Transition Metal Oxides as Cathode for Rechargeable Sodium Batteries Prepared by Higherature Calcination. *ACS Appl. Mater. Interfaces* **2014**, *6*, 17176−17183.

(12) Shen, Y.; Birgisson, S.; Iversen, B. B. A P2-$Na_x$ $Co_{0.7}$ $Mn_{0.3}$ $O_2$ (X ≈ 1.0) Cathode Material for Na-Ion Batteries with Superior Rate and Cycle Capability. *J. Mater. Chem. A* **2016**, *4*, 12281−12288.

(13) Ramasamy, H. V.; Kaliyappan, K.; Thangavel, R.; Aravindan, V.; Kang, K.; Sun, X.; Lee, Y.-S.; Kim, D. U.; Park, Y. Cu-Doped P2-Na0.5Ni0.33Mn0.67O2 Encapsulated with MgO as Novel High Voltage Cathode with Enhanced Na-Storage Properties. *J. Mater. Chem. A* **2017**, *5*, 8408−8415.

(14) Hemalatha, K.; Jayakumar, M.; Bera, P.; Prakash, A. S. Improved Electrochemical Performance of Na 0.67 MnO 2 through Ni and Mg Substitution. *J. Mater. Chem. A* **2015**, *3*, 20908−20912.

(15) Yabuuchi, N.; Kajiyama, M.; Iwatate, J.; Nishikawa, H.; Hitomi, S.; Okuyama, R.; Usui, R.; Yamada, Y.; Komaba, S. P2-Type Nax[Fe1/2Mn1/2]O2Made from Earth-Abundant Elements for Rechargeable Na Batteries. *Nat. Mater.* **2012**, *11*, 512−517.

(16) Wang, X.; Tamaru, M.; Okubo, M.; Yamada, A. Electrode Properties of P2−Na 2/3 Mn Y Co 1− Y O 2 as Cathode Materials for Sodium-Ion Batteries. *J. Phys. Chem. C* **2013**, *117*, 15545−15551.

(17) Li, Y.; Yang, Z.; Xu, S.; Mu, L.; Gu, L.; Hu, Y.-S.; Li, H.; Chen, L. Air-Stable Copper-Based P2-Na7/9Cu2/9Fe1/9Mn2/3O2 as a New Positive Electrode Material for Sodium-Ion Batteries. *Adv. Sci.* **2015**, *2*, 1500031.

(18) Lim, S.-J.; et al. Structural Enhancement of Na3V2(PO4)3/C Composite Cathode Materials by Pillar Ion Doping for High Power and Long Cycle Life Sodium-Ion Batteries. *J. Mater. Chem. A* **2014**, *2*, 19623−19632.

(19) Hasa, I.; Passerini, S.; Hassoun, J. Toward High Energy Density Cathode Materials for Sodium-Ion Batteries: Investigating the Beneficial Effect of Aluminum Doping on the P2-Type Structure. *J. Mater. Chem. A* **2017**, *5*, 4467−4477.

(20) Bucher, N.; Hartung, S.; Franklin, J. B.; Wise, A. M.; Lim, L. Y.; Chen, H. Y.; Weker, J. N.; Toney, M. F.; Srinivasan, M. P2-NaxCoyMn1-yO2 (Y = 0, 0.1) as Cathode Materials in Sodium-Ion Batteries - Effects of Doping and Morphology to Enhance Cycling Stability. *Chem. Mater.* **2016**, *28*, 2041−2051.

(21) Liu, Y.; Fang, X.; Zhang, A.; Shen, C.; Liu, Q.; Enaya, H. A.; Zhou, C. Layered P2-Na2/3[Ni1/3Mn2/3]O2 as High-Voltage Cathode for Sodium-Ion Batteries: The Capacity Decay Mechanism and Al2O3 Surface Modification. *Nano Energy* **2016**, *27*, 27−34.

(22) Wu, X.; Guo, J.; Wang, D.; Zhong, G.; McDonald, M. J.; Yang, Y. P2-Type Na0.66Ni0.33-xZnxMn0.67O2 as New High-Voltage Cathode Materials for Sodium-Ion Batteries. *J. Power Sources* **2015**, *281*, 18−26.

(23) Fang, C.; Huang, Y.; Zhang, W.; Han, J.; Deng, Z.; Cao, Y.; Yang, H. Routes to High Energy Cathodes of Sodium-Ion Batteries. *Adv. Energy Mater.* **2016**, *6*, 1501727.

(24) Billaud, J.; Singh, G.; Armstrong, A. R.; Gonzalo, E.; Roddatis, V.; Armand, M.; Rojo, T.; Bruce, P. G. Na0.67Mn1−xMgxO2 (0 ≤ X ≤ 0.2): A High Capacity Cathode for Sodium-Ion Batteries. *Energy Environ. Sci.* **2014**, *7*, 1387−1391.

(25) Clément, R.; Billaud, J.; Armstrong, A. R.; Singh, G.; Rojo, T.; Bruce, P. G.; Grey, C. P. Structurally Stable Mg-Doped P2-Na 2/3 Mn 1-Y Mg Y O 2 Sodium-Ion Battery Cathodes with High Rate Performance: Insights from Electrochemical, NMR and Diffraction Studies. *Energy Environ. Sci.* **2016**, *9*, 3240−3251.




DOI: 10.1021/acs.jpclett.7b02012
*J. Phys. Chem. Lett.* 2017, 8, 5021−5030

(26) Wang, P. F.; You, Y.; Yin, Y. X.; Wang, Y. S.; Wan, L. J.; Gu, L.; Guo, Y. G. Suppressing the P2-O2 Phase Transition of Na0.67Mn0.67Ni0.33O2 by Magnesium Substitution for Improved Sodium-Ion Batteries. *Angew. Chem., Int. Ed.* **2016**, *55*, 7445−7449.
(27) Kaliyappan, K.; Liu, J.; Lushington, A.; Li, R.; Sun, X. Highly Stable $Na_{2/3}(Mn_{0.54}Ni_{0.13}Co_{0.13})O_2$ Cathode Modified by Atomic Layer Deposition for Sodium Ion Batteries by Atomic Layer Deposition for Sodium-Ion Batteries. *ChemSusChem* **2015**, *8*, 2537−2543.
(28) Zhan, D.; Liang, Y.; Cui, P.; Xiao, Z. Al-Doped LiMn2O4 Single Crystalline Nanorods with Enhanced Elevated-Temperature Electrochemical Performance via a Template-Engaged Method as a Cathode Material for Lithium Ion Batteries. *RSC Adv.* **2015**, *5*, 6372−6377.
(29) Zhu, Y.-E.; Qi, X.; Chen, X.; Zhou, X.; Zhang, X.; Wei, J.; Hu, Y.; Zhou, Z.; Bruce, P. G.; Scrosati, B.; et al. A P2-$Na_{0.67}$ $Co_{0.5}$ $Mn_{0.5}$ $O_2$ Cathode Material with Excellent Rate Capability and Cycling Stability for Sodium Ion Batteries. *J. Mater. Chem. A* **2016**, *4*, 11103−11109.
(30) Carlier, D.; Cheng, J. H.; Berthelot, R.; Guignard, M.; Yoncheva, M.; Stoyanova, R.; Hwang, B. J.; Delmas, C. The P2-Na(2/3)Co(2/3)Mn(1/3)O2 Phase: Structure, Physical Properties and Electrochemical Behavior as Positive Electrode in Sodium Battery. *Dalton Trans.* **2011**, *40*, 9306−9312.
(31) Li, Z.-Y.; Gao, R.; Zhang, J.; Zhang, X.; Hu, Z.; Liu, X. New Insights into Designing High-Rate Performance Cathode Materials for Sodium Ion Batteries by Enlarging the Slab-Spacing of the Na-Ion Diffusion Layer. *J. Mater. Chem. A* **2016**, *4*, 3453−3461.
(32) Li, Z.-Y.; Zhang, J.; Gao, R.; Zhang, H.; Hu, Z.; Liu, X. Unveiling the Role of Co in Improving the High-Rate Capability and Cycling Performance of Layered $Na_{0.7}$ $Mn_{0.7}$ $Ni_{0.3-X}$ $Co_X$ $O_2$ Cathode Materials for Sodium-Ion Batteries. *ACS Appl. Mater. Interfaces* **2016**, *8*, 15439−15448.
(33) Fouassier, C.; et al. Sur de Nouveaux Bronzes Oxyg6n6s de Formule $Na_\chi CoO2$ ($\chi$ < l). Le Système Cobalt-Oxygène-Sodium. *J. Solid State Chem.* **1973**, *6*, 532−537.
(34) Chen, X.; Zhou, X.; Hu, M.; Liang, J.; Wu, D.; Wei, J.; Zhou, Z. Stable Layered P3/P2 $Na_{0.66}$ $Co_{0.5}$ $Mn_{0.5}$ $O_2$ Cathode Materials for Sodium-Ion Batteries. *J. Mater. Chem. A* **2015**, *3*, 20708−20714.
(35) He, Y.; Li, H.; Ou, L.; Ding, F.; Zhan, Z.; Zhong, Y. Preparation and Characterisation of Water-Based Aluminium Pigments Modified with SiO2 and Polymer Brushes. *Corros. Sci.* **2016**, *111*, 802−810.
(36) Li, Z.-Y.; Gao, R.; Sun, L.; Hu, Z.; Liu, X. Designing an Advanced P2-Na 0.67 Mn 0.65 Ni 0.2 Co 0.15 O 2 Layered Cathode Material for Na-Ion Batteries. *J. Mater. Chem. A* **2015**, *3*, 16272−16278.
(37) Nayak, P. K.; Grinblat, J.; Levi, M.; Levi, E.; Kim, S.; Choi, J. W.; Aurbach, D. Al Doping for Mitigating the Capacity Fading and Voltage Decay of Layered Li and Mn-Rich Cathodes for Li-Ion Batteries. *Adv. Energy Mater.* **2016**, *6*, 1502398.
(38) Xiao, L.; Zhao, Y.; Yang, Y.; Cao, Y.; Ai, X.; Yang, H. Enhanced Electrochemical Stability of Al-Doped $LiMn_2O_4$ Synthesized by a Polymer-Pyrolysis Method. *Electrochim. Acta* **2008**, *54*, 545−550.
(39) Wang, L.; Sun, Y.-G.; Hu, L.-L.; Piao, J.-Y.; Guo, J.; Manthiram, A.; Ma, J.; Cao, A.-M. Copper-Substituted Na0.67Ni0.3-xCuxMn0.7O2 Cathode Materials for Sodium-Ion Batteries with Suppressed P2-O2 Phase Transition. *J. Mater. Chem. A* **2017**, *5*, 8752−8761.
(40) Karthikeyan, K.; Amaresh, S.; Kim, S. H.; Aravindan, V.; Lee, Y. S. Influence of Synthesis Technique on the Structural and Electrochemicalproperties Of "cobalt-Free", Layered Type Li 1+x-(Mn0.4Ni0.4Fe0.2) 1-xO2(0 < X < 0.4) Cathode Material for Lithium Secondary Battery. *Electrochim. Acta* **2013**, *108*, 749−756.
(41) Karthikeyan, K.; Amaresh, S.; Lee, G. W.; Aravindan, V.; Kim, H.; Kang, K. S.; Kim, W. S.; Lee, Y. S. Electrochemical Performance of Cobalt Free, Li1.2(Mn0.32Ni0.32Fe0.16)O2 Cathodes for Lithium Batteries. *Electrochim. Acta* **2012**, *68*, 246−253.
(42) Zhou, W. J.; Bao, S. J.; He, B. L.; Liang, Y. Y.; Li, H. L. Synthesis and Electrochemical Properties of LiAl0.05Mn1.95O4 by the Ultrasonic Assisted Rheological Phase Method. *Electrochim. Acta* **2006**, *51*, 4701−4708.
(43) Okada, M.; Lee, Y.; Yoshio, M. Cycle characterizations of LiMxMn2−xO4 (M=Co, Ni) materials for lithium secondary battery at wide voltage region. *J. Power Sources* **2000**, *90*, 196−200.
(44) Liu, S.; Jiang, X.; Zhang, J.; Yang, J.; Qian, Y. Design and Synthesis of a Stable-Performance P2- Type Layered Cathode Material for Sodium Ion Batteries. *RSC Adv.* **2016**, *6*, 55327−55330.
(45) Ceder, G.; Sadoway, D. R.; Aydinol, M. K.; Huang, B.; et al. Identification of Cathode Materials for Lithium Batteries Guided by First-Principles Calculations. *Nature* **1998**, *392*, 694−696.
(46) Levi, M. D.; Dargel, V.; Shilina, Y.; Aurbach, D.; Halalay, I. C. Impedance Spectra of Energy-Storage Electrodes Obtained with Commercial Three-Electrode Cells: Some Sources of Measurement Artefacts. *Electrochim. Acta* **2014**, *149*, 126−135.
(47) Rani, J. R.; Thangavel, R.; Oh, S.-I.; Woo, J. M.; Chandra Das, N.; Kim, S.-Y.; Lee, Y.-S.; Jang, J.-H. High Volumetric Energy Density Hybrid Supercapacitors Based on Reduced Graphene Oxide Scrolls. *ACS Appl. Mater. Interfaces* **2017**, *9*, 22398−22407.
(48) Kalluri, S.; Seng, K. H.; Pang, W. K.; Guo, Z.; Chen, Z.; Liu, H. K.; Dou, S. X. Electrospun P2 Type Na2/3(Fe1/2Mn1/2)O2 Hierarchial Nanofibers as Cathode Material For Sodium Ion Batteries. *ACS Appl. Mater. Interfaces* **2014**, *6*, 8953−8958.
(49) Bai, Y.; Zhao, L.; Wu, C.; Li, H.; Li, Y.; Wu, F. Enhansed Sodium Ion Storage Behaviour of P2 Type Na2/3Fe1/2Mn1/2O2 Synthesized via a Chelating Agent Assisted Route. *ACS Appl. Mater. Interfaces* **2016**, *8*, 2857−2865.


DOI: 10.1021/acs.jpclett.7b02012
*J. Phys. Chem. Lett.* 2017, 8, 5021−5030